Article

Synchrotron infrared spectroscopic evidence of the probable transition to metal hydrogen

https://doi.org/10.1038/s41586-019-1927-3

Received: 12 April 2019

Accepted: 26 November 2019

Published online: 29 January 2020

Paul Loubeyre[1]*, Florent Occelli[1] & Paul Dumas[1,2]

Hydrogen has been an essential element in the development of atomic, molecular and condensed matter physics[1]. It is predicted that hydrogen should have a metal state[2]; however, understanding the properties of dense hydrogen has been more complex than originally thought, because under extreme conditions the electrons and protons are strongly coupled to each other and ultimately must both be treated as quantum particles[3,4]. Therefore, how and when molecular solid hydrogen may transform into a metal is an open question. Although the quest for metal hydrogen has pushed major developments in modern experimental high-pressure physics, the various claims of its observation remain unconfirmed[5–7]. Here a discontinuous change of the direct bandgap of hydrogen, from 0.6 electronvolts to below 0.1 electronvolts, is observed near 425 gigapascals. This result is most probably associated with the formation of the metallic state because the nucleus zero-point energy is larger than this lowest bandgap value. Pressures above 400 gigapascals are achieved with the recently developed toroidal diamond anvil cell[8], and the structural changes and electronic properties of dense solid hydrogen at 80 kelvin are probed using synchrotron infrared absorption spectroscopy. The continuous downward shifts of the vibron wavenumber and the direct bandgap with increased pressure point to the stability of phase-III hydrogen up to 425 gigapascals. The present data suggest that metallization of hydrogen proceeds within the molecular solid, in good agreement with previous calculations that capture many-body electronic correlations[9].

The search for metal hydrogen has a unique place in high-pressure physics. Indisputably, metal hydrogen should exist. Owing to increase in electron kinetic energy because of quantum confinement, pressure should turn any insulator into a metal, as observed for molecular oxygen around 100 GPa some 20 years ago[10]. At first, the prediction of the insulator–metal transition in dense hydrogen was intertwined with the molecular dissociation[2]. However, it was later suggested that metal hydrogen may exist as a proton-paired metal[11]. Quantitative predictions of the stability domain and of the properties of metal hydrogen remain challenging because many contributions could be in effect and should be self-consistently treated[3,4]; for example, many-body electronic correlations, nuclear quantum effects, nuclear spin ordering, coupling between protons and electrons (as suggested by a large Born–Oppenheimer separation parameter), or anharmonic effects. The most advanced calculations, such as diffusion Monte Carlo (DMC) simulations[4,9,12], now go beyond the electronic correlation mean-field description of density functional theory and try to capture many-body electronic correlations. Importantly, metal hydrogen should exhibit notable properties, such as room-temperature superconductivity[13–15], a melting transition at a very low temperature into a superconducting superfluid state[16] and a mobile solid state[17].

The change in the direct bandgap of solid hydrogen was previously measured up to 300 GPa by visible absorption mesurements[18]. By extrapolating to zero the linear decrease of the bandgap with density, the transition to metal hydrogen was predicted to occur around 450 GPa. In this work, we extend the investigation of the direct bandgap decrease down to the near-to-mid-infrared energy range. Infrared measurements provide a non-intrusive method both to disclose structural changes and also to characterize the electronic properties of hydrogen up to its metal transition. Our approach is based on two experimental developments. First, in order to overcome the 400 GPa limit of conventional diamond anvil cells[19], we used the recently developed toroidal diamond anvil cell (T-DAC)[8] that can achieve pressures of up to 600 GPa. Importantly, under extreme pressures, the T-DAC preserves the advantages of the standard diamond anvil cell in terms of stress distribution, optical access and sample size. Synthetic type-IIa diamond anvils were used to provide infrared transparency down to 800 cm^{-1}. Second, an infrared horizontal microscope was designed to be coupled to a collimated exit port of a synchrotron-feed Fourier-transform infrared spectrometer at the SMIS beamline at the SOLEIL synchrotron facility. Such a high-brightness broadband infrared source is essential for measuring, by transmission, satisfactory signal-to-noise

[1]CEA, DAM, DIF, Arpajon, France. [2]Synchrotron SOLEIL, Gif-sur-Yvette, France. *e-mail: paul.loubeyre@cea.fr

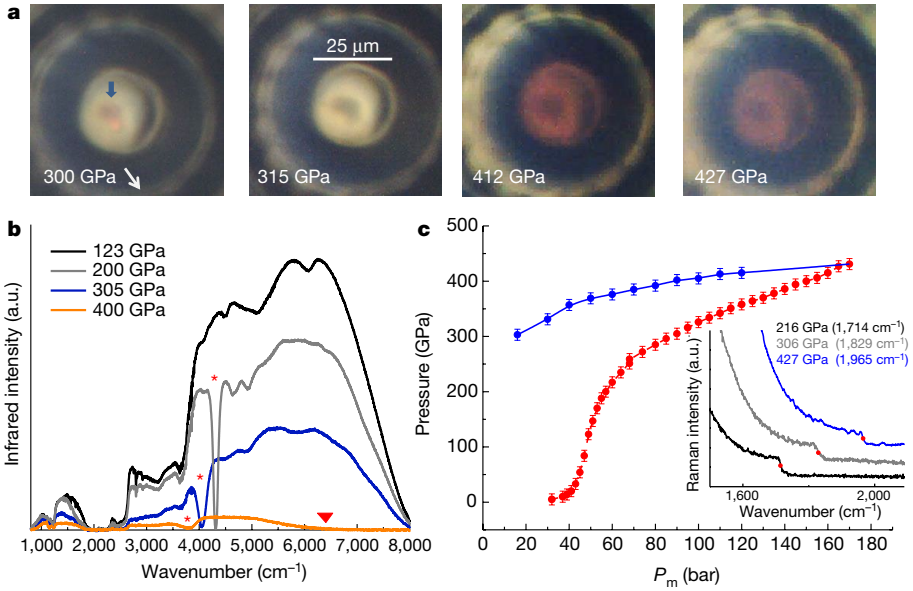

Fig. 1 | A selection of measurements over the investigated pressure range. **a**, Photographs of the hydrogen sample taken at different stages of compression, under simultaneous front and back bright-light illumination. The hydrogen sample is indicated by the blue arrow. Around 310 GPa, the sample reversibly turns black, as illustrated by the photographs taken at 315 GPa for the increasing pressure path and at 300 GPa for the decreasing pressure path. At 427 GPa, the sample is in the metallic state and is still distinguishable from the rhenium gasket. The red-coloured aspect at the diamond tip centre is attributed to the decrease of the diamond bandgap[8]. **b**, Infrared transmission spectra at various pressures. Intrinsic absorption features associated with the vibron and with the closing of the bandgap are indicated by the red stars and the triangle, respectively. **c**, Pressure evolution in hydrogen versus the helium membrane pressure acting on the piston of the T-DAC, during pressure increase (red) and decrease (blue). Inset, the high-wavenumber part of the Raman diamond spectra collected at three pressures. The wavenumber at the step used to calculate pressure is indicated as a red dot, and noted in the key. Solid lines are guides to the eye. a.u., arbitrary units.

ratio spectra through a 5-μm diameter sample. Simultaneous Raman spectroscopy and visual observation could be performed.

Figure 1 illustrates selected data obtained for the hydrogen sample in the T-DAC at 80 K during different compression and decompression stages. Four photographs (Fig. 1a) show the changes in the sample appearance. The formation of black hydrogen—that is, the transformation of hydrogen from transparent to totally opaque in the visible range—is observed around 310 GPa, as previously reported[18], and this was reversible upon pressure release. The visual transformation of the sample at the probable insulator–metal transition is less contrasted. The observed metal-hydrogen sample is not highly reflective, as it appears darker than the surrounding rhenium gasket. As discussed below, this is consistent with the formation of a molecular metal instead of an atomic metal. The infrared signal was collected over the 800–8,000 cm^{-1} wavenumber range; several raw spectra are shown in Fig. 1b. Up to 360 GPa, the signal intensity decreased owing to the shrinkage of the hydrogen sample size and the deformation of the toroidal anvil tip[8]. However, after intensity normalization, from 123 GPa to 360 GPa all spectra display the same shape when the hydrogen vibron peak is discarded (see Extended Data Fig. 1). Consequently, the variation of the infrared transmittance of the diamond anvil itself should remain negligible up to the 400 GPa range. Therefore changes in the infrared spectra can only be due to intrinsic properties of hydrogen. In Fig. 1a, two interesting features are clearly seen: (1) the strong absorption peak around 4,000 cm^{-1} is associated with the H_2 vibron that appears above 160 GPa upon the solid entering phase III, as reported previously[20]. This vibron mode broadens and shifts to lower wavenumbers with increasing pressure; (2) above 360 GPa, the shape of the infrared spectra display zeroing at high wavenumbers, evolving towards low values with pressure (see Extended Data Fig. 2), which indicates the decrease of the hydrogen direct bandgap in the infrared range. Importantly, a very discernible Raman diamond edge (see inset Fig. 1c), used as the pressure gauge, could be measured up to the maximum pressure and upon release, as a result of an elastic deformation at the diamond anvil tip facilitated by the toroidal shape. In Fig. 1c, the evolution of the sample pressure versus the force on the piston features the expected trend[8,19].

In Fig. 2a, absorbance spectra have been obtained by taking a direct ratio of the spectrum at a given pressure to that taken at 123 GPa (after intensity normalization). For infrared measurements of semiconductors under pressure, the direct excitonic level (in the case of hydrogen, the values of the excitonic and of the direct bandgap should be almost identical)[21] is positioned at the junction between the absorbance plateau and the lower energy tail, as done previously to position the hydrogen bandgap in the visible range[18]. In the present experimental configuration, a maximum absorbance value of just 2 could be measured. Hence, a lower bound for the bandgap should probably be inferred because the absorbance plateau might be at a higher value. However, because the hydrogen sample was about 1.6 (± 0.1) μm thick, the absorption coefficient associated with an absorbance of 2 is estimated to be about 28,000 cm^{-1}, which is similar to the value obtained from the direct bandgap measurements in the visible range[18]. The bandgap underestimation should be smaller than 0.14 eV. Around 425 GPa, a transition to a total infrared absorption is observed, corresponding to an absorption coefficient greater than 25,000 cm^{-1} over the whole infrared spectral range investigated. This is a necessary condition for the infrared observation of metal hydrogen but not definitive evidence, because the existence of a direct bandgap less than 0.1 eV—that is, below the 800 cm^{-1} lower limit of the covered infrared spectral range—cannot be ruled out, although that seems unlikely because the nucleus zero-point energy is greater than this value. In Fig. 2c, the discontinuity of the transition is evidenced by the pressure evolution of the integrated infrared intensity over the 800–2,000 cm^{-1} wavenumber range. Upon pressure release, the infrared spectral intensity and shape are reversibly recovered (see Extended Data Fig. 2). The *C*2/*c* structure with 24 atoms per unit cell, henceforth *C*2/*c*-24, has been calculated to be the most probable candidate in the pressure range of the present measurements[22]. If so, from electronic band structure calculations[21], an indirect bandgap should close under pressure before the direct bandgap does. Consistent with

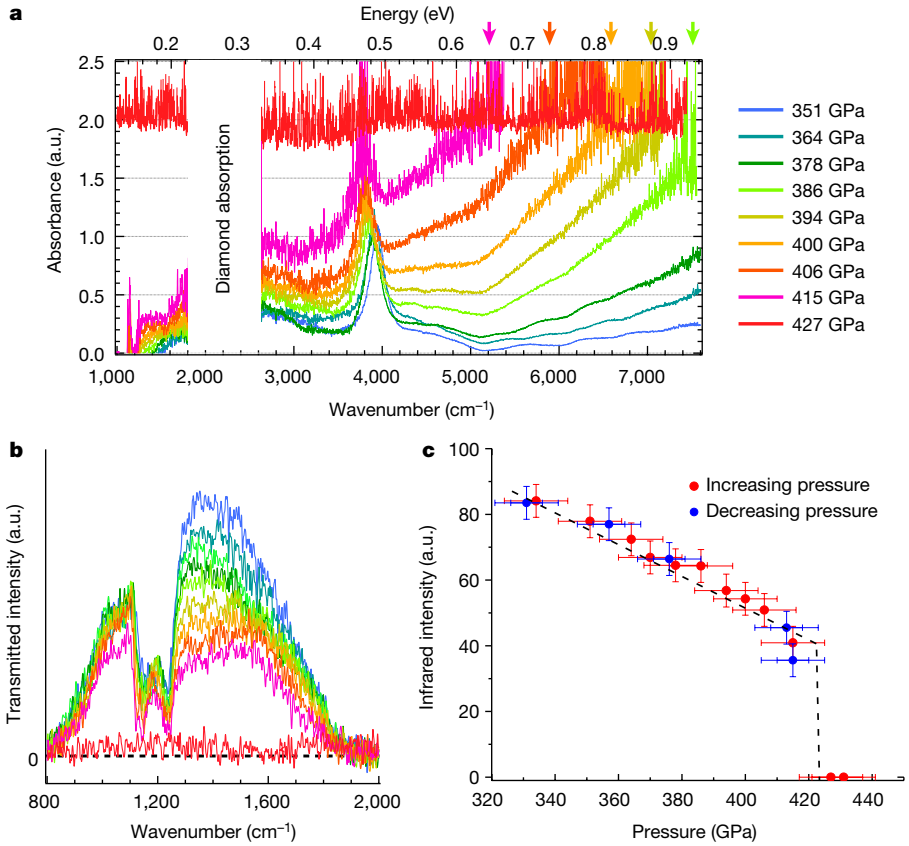

Fig. 2 | Discontinuous pressure evolution in the infrared absorption and probable signature of metal hydrogen. a, Absorption spectra of hydrogen at different pressures. Above 386 GPa, the direct electronic bandgap is indicated by arrows. For clarity, different colours are associated with different pressures. **b**, Transmission spectra over the infrared range 800–2,000 cm^{-1}. The pressure colourscale is as in **a**. **c**, Integrated transmitted intensity over the 800–2,000 cm^{-1} infrared range for increasing (red) and decreasing (blue) pressure. Pressure uncertainty is ±10 GPa. Errors are the random uncertainty estimated from different measurements at the same pressure, for typically three measurements. The dashed lines in **b**, **c** are guides to the eye.

this picture, hydrogen was recently reported[23] to start conducting above 350 GPa (or 330 GPa, if the diamond pressure scale used here is applied). Then up to 440 GPa (or 395 GPa in our case), the value of the resistivity (about 5×10^{-4} Ω m), and its temperature dependence suggest a semimetal state with a low concentration of charge carriers. The associated plasma edge should be below 0.1 eV, which is why it could not be detected here. For comparison, the plasma edge of the low-density charge carriers conducting xenon could only be measured using the present synchrotron infrared setup[24] just above the xenon metallization pressure when the resistivity falls below 1×10^{-4} Ω m (ref. [23]).

Properties of solid hydrogen up to the metal transition are shown in Fig. 3. In Fig. 3a, the linear pressure shift of the vibron wavenumber from 160 GPa to 425 GPa indicates that no structural change occurs up to 425 GPa and that the solid hydrogen remains in phase III. The *C*2/*c*-24 candidate structure for phase III was first proposed using an ab initio random structure searching method[22]. It consists of layers of molecules forming a slight monoclinic distortion of the hexagonal lattice. The *C*2/*c*-24 structure has a specific infrared fingerprint[22], exhibiting one intense vibron infrared mode as well as one intense phonon infrared mode, in good agreement with the present observation. The phonon mode is, to our knowledge, reported here for the first time but could be observed only up to 225 GPa, above which it becomes hidden by the strong absorption of the diamond anvils. The vibron wavenumber shift was reversibly observed upon pressure decrease (see Extended Data Fig. 3). Finally, the calculated[22,25] pressure evolutions of the vibron and of the phonon infrared wavenumbers for the *C*2/*c*-24 structure are in very good agreement with the present experimental data. In Fig. 3b, the direct bandgap is seen to decrease linearly with pressure, and is well matched with the previous measurements in the visible range[18]. In calculations, the bandgap is profoundly affected by the level of the description of electronic exchange–correlation and also by nuclear quantum effects. Previous work that has used local exchange–correlation density functional theory, for example using the Perdew–Burke–Ernzerhof (PBE) calculation[21] or implementing vdW-DF2[26], has obtained unreliable bandgaps, and has usually underestimated its value. The more advanced methods of quasi-particle computational approaches, GW[22] and DMC[9], should be more reliable. In Fig. 3b, they are seen to give higher bandgap values than obtained by experiment. Accounting for nuclear quantum effects should lower the bandgap energy[26] by at least 1 eV and therefore a better agreement with the present data should be obtained. It is interesting to note that there is a confluence of the bandgap and of the vibron energy values, both about 0.5 eV, when the transition to the probable metal state occurs.

Currently, there are five experimentally described phases of hydrogen[4,27]. Recently, a single crystal X-ray diffraction study[28] at 300 K up to 254 GPa showed that the I, III and IV phases are isostructural, and the hydrogen molecules remain in the hexagonal close-packed crystal lattice structure. Phases IV and V exist only above 200 K (refs. [23,27]). An updated low-temperature phase diagram of solid hydrogen is shown in Fig. 4. In phase I, the molecules are in a quantum free-rotational state and arranged on a hexagonal close-packed lattice. Upon transitioning to phase II, very small discontinuities in the lattice parameters have been measured[29]. Quantum molecular rotations become restricted and phase II can be described as a quantum fluxional solid[30]. At 160 GPa, phase II transforms into an ordered molecular phase III. We suggest here that phase III has the *C*2/*c*-24 structure up to 425 GPa, above which a discontinuous transition to metal hydrogen occurs. It should be noted that the infrared spectra in phase III at 300 K and at 100 K are reasonably

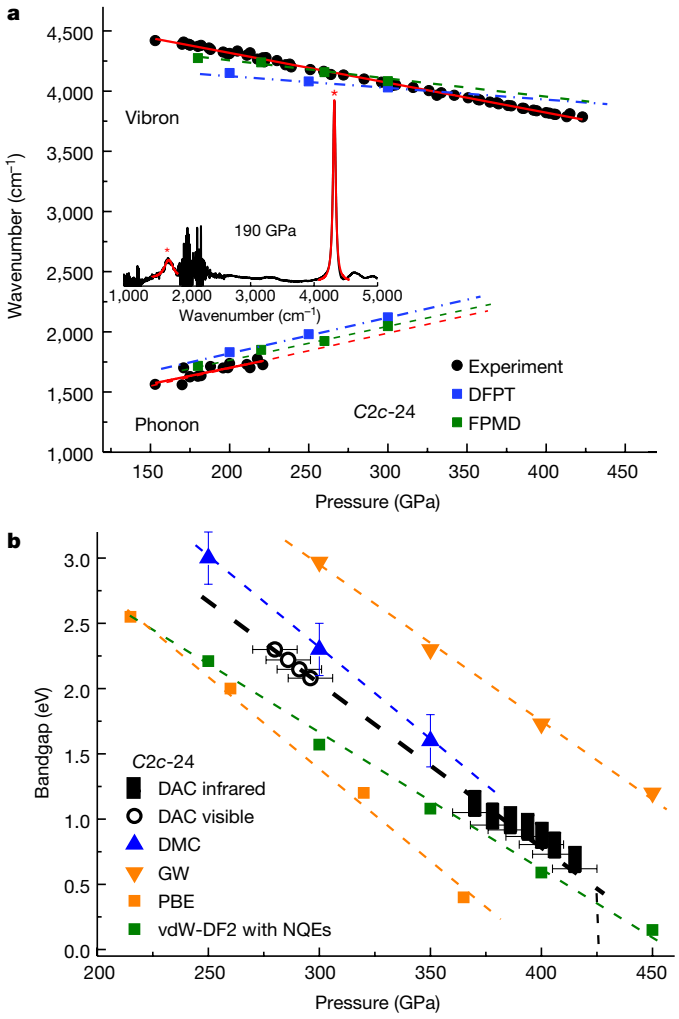

Fig. 3 | Evolution of the molecular solid hydrogen properties up to the insulator–metal transition: comparison between experiment and calculations. a, Wavenumbers of the vibron and of the phonon infrared active modes in phase III versus pressure. The black dots and the red lines represent experimental data and linear fits. The blue squares and the green triangles are the density functional perturbation theory[21] and first-principles molecular dynamics[25] calculations for the *C*2/*c*-24 structure, respectively. Inset, the infrared absorption spectrum at 190 GPa, showing the vibron and the phonon peaks. Comparison of the present data with previous experimental determinations of the infrared H_2 vibron wavenumber versus pressure is shown in Extended Data Fig. 4. **b**, The pressure evolution of the experimental bandgap (combining data in the visible range[18] and the present infrared data; black symbols), is compared to calculations for the *C*2/*c*-24 structure performed under a variety of approximations: within the DFT framework with local PBE (orange squares) and nonlocal vdW-DF2 (green squares) exchange–correlation functionals[26]; with the quasiparticle approach within the GW approximation[9] (orange triangles); and with the DMC method[22] (blue triangles). The vertical dashed line indicates the transition to metal hydrogen. The uncertainty on the bandgap is 0.14 eV, estimated from Fig. 2a by linearly extending the rising absorbance before the plateau of 2 to an absorbance value of 3. The dashed lines that follow the data are guides to the eye. Evolution of the direct bandgap versus density, using a revisited hydrogen compression curve to convert pressure into density, is shown in Extended Data Fig. 5. Vibron and bandgap data are presented in Extended Data Table 1.

different and are associated with a substantial temperature shift of the vibron wavenumber[31]. The orientational ordering of the molecules could be increased by lowering the temperature, hence inducing the monoclinic distortion from the hexagonal close-packed lattice at 300 K to form the *C*2/*c*-24 structure at 80 K. In the framework of PBE density functional theory, the *C*2/*c*-24 structure should be stable only up to

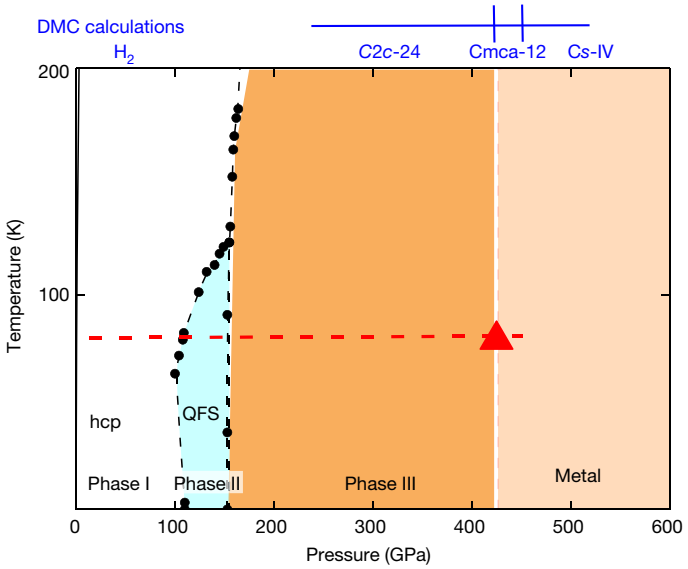

Fig. 4 | Low-temperature phase diagram of solid hydrogen. The red dashed line is the pathway of the infrared data collection and the red triangle indicates the transition to metal hydrogen. Boundary lines between phases I, II and III are from previous studies (as reviewed in ref. [4]). The sequence of phase transitions, determined by DMC calculations including nuclear quantum effects[9], is displayed at the top of the graph.

270 GPa[21]. Using DMC calculations and including nuclear quantum effects, a transition from an insulating *C*2/*c*-24 structure to a metallic *Cmca*-12 structure is obtained at 424 GPa[9], in good agreement with the pressure at which we observe total infrared absorption above 800 cm^{-1}. That structural transition should be displacive, implying an orientation ordering in the layers of the H_2 molecules from nearly parallel to flat, which should induce a larger distortion from hexagonal packing. That could take place with almost no pressure hysteresis. Furthermore, the reflectivity in the visible range for the *Cmca*-12 molecular metal has been calculated[32] to be about 0.5, and so this molecular metal should appear darker than the rhenium gasket. Consequently, the full infrared absorption, the small hysteresis of the transition and the photograph of the sample above 425 GPa all suggest that we have observed the hydrogen insulator-to-metal transition in the molecular crystal, associated with a structural transition from *C*2/*c*-24 to *Cmca*-12. Following DMC calculations[9], atomic metal hydrogen should be observed above 447 GPa.

More measurements are now needed to definitively prove the hydrogen transition to a metallic state. It seems particularly appropriate to try to observe the predicted high-temperature superconductivity of metal hydrogen in both the molecular and atomic hydrogen-metal phases, at 250 K (ref. [14]) and 350 K (ref. [15]), respectively. For doing so, a non-invasive infrared reflectivity measurement has recently been proposed[33], and the sample size reachable using the T-DAC will improve our ability to make such a measurement.

Online content

Any methods, additional references, Nature Research reporting summaries, source data, extended data, supplementary information, acknowledgements, peer review information; details of author contributions and competing interests; and statements of data and code availability are available at https://doi.org/10.1038/s41586-019-1927-3.

1. Rigden, J. S. *Hydrogen, the Essential Element* (Harvard Univ. Press, 2002).
2. Wigner, E. & Huntington, H. B. On the possibility of a metallic modification of hydrogen. *J. Chem. Phys.* **3**, 764–770 (1935).
3. Ashcroft, N. Dense hydrogen: the reluctant alkali. *Phys. World* **8**, 43–48 (1995).
4. McMahon, J. M., Morales, M. A., Pierleoni, C. & Ceperley, D. M. The properties of hydrogen and helium under extreme conditions. *Rev. Mod. Phys.* **84**, 1607–1653 (2012).

5. Mao, H. K. & Hemley, R. J. Optical studies of hydrogen above 200 gigapascals: evidence for metallization by band overlap. *Science* **244**, 1462–1465 (1989).
6. Eremets, M. I. & Troyan, I. A. Conductive dense hydrogen. *Nat. Mater.* **10**, 927–931 (2011).
7. Dias, R. P. & Silvera, I. F. Observation of the Wigner–Huntington transition to metallic hydrogen. *Science* **355**, 715–718 (2017).
8. Dewaele, A., Loubeyre, P., Occelli, F., Marie, O. and Mezouar, M. Toroidal diamond anvil cell for detailed measurements under extreme static pressures. *Nat. Commun.* **9**, 2913 (2018).
9. McMinis, J., Clay III, R.C., Lee, D. and Morales, M. A. Molecular to atomic phase transition in hydrogen under high pressure. *Phys. Rev. Lett.* **114**, 105305 (2015).
10. Desgreniers, S., Vohra, Y. K. & Ruoff, A. L. Optical response of very high density solid oxygen to 132 GPa. *J. Phys. Chem.* **94**, 1117–1122 (1990).
11. Johnson, K. A. & Ashcroft, N. W. Structure and bandgap closure in dense hydrogen. *Nature* **403**, 632–635 (2000).
12. Drummond, N.D. et al. Quantum Monte Carlo study of the phase diagram of solid molecular hydrogen at extreme pressures. *Nat. Commun.* **6**, 7794 (2015).
13. Ashcroft, N. W. Metallic hydrogen: a high-temperature superconductor? *Phys. Rev. Lett.* **21**, 1748–1749 (1968).
14. Cudazzo, P. et al. Ab initio description of high temperature superconductivity in dense molecular hydrogen. *Phys. Rev. Lett.* **100**, 257001 (2008).
15. Borinaga, M., Errea, I., Calandra, M., Mauri, F. & Bergara, A. Anharmonic effects in atomic hydrogen: superconductivity and lattice dynamical stability. *Phys. Rev. B* **93**, 174308 (2016).
16. Babaev, E., Sudbo, A. and Ashcroft, N.W. Observability of a new state of matter: a metallic superfluid. *Phys. Rev. Lett.* **95**, 105301 (2005).
17. Geng, H. Y., Wu, Q. & Sun, Y. Prediction of a mobile solid state in dense hydrogen under high pressures. *J. Phys. Chem. Lett.* **8**, 223–228 (2017).
18. Loubeyre, P., Occelli, F. & LeToullec, R. Optical studies of solid hydrogen to 320 GPa and evidence for black hydrogen. *Nature* **416**, 613–617 (2002).
19. Li, B. et al. Diamond anvil cell behavior up to 4 Mbar. *Proc. Natl Acad. Sci. USA* **115**, 1713–1717 (2018).
20. Hanfland, M., Hemley, R. J. & Mao, H. K. Novel infrared vibron absorption of solid hydrogen at megabar pressures. *Phys. Rev. Lett.* **70**, 3760–3763 (1993).
21. Azadi, M., Drummond, N. D. & Foulkes, W. M. C. Nature of the metallization transition in solid hydrogen. *Phys. Rev. B* **95**, 035142 (2017).
22. Pickard, C. J. & Needs, R.J. Structure of phase III of solid hydrogen. *Nat. Phys.* **3**, 473–476 (2007).
23. Eremets, M. I., Drozdov, A. P., Kong, P. P. & Wang, H. Semimetallic molecular hydrogen at pressure above 350 GPa. *Nat. Phys.* **15**, 1246–1249 (2019).
24. Dewaele, A., Loubeyre, P., Dumas, P. and Mezouar, M. Oxygen impurities reduce the metallization pressure of xenon. *Phys. Rev. B* **86**, 014103 (2012).
25. Zhang, C. et al. Finite-temperature infrared and Raman spectra of high-pressure hydrogen from first-principle molecular dynamics. *Phys. Rev. B* **98**, 144301 (2018).
26. Morales, M., Mc Mahon, J. M., Pierleoni, C. & Ceperley, D. M. Towards a predictive first-principles description of solid molecular hydrogen with density functional theory. *Phys. Rev. B* **87**, 184107 (2013).
27. Dalladay-Simpson, P., Howie, R. T. & Gregoryanz, E. Evidence for a new phase of dense hydrogen above 325 gigapascals. *Nature* **529**, 63–67 (2016).
28. Ji, C. et al. Ultrahigh-pressure isostructural electronic transitions in hydrogen. *Nature* **573**, 558–562 (2019).
29. Goncharenko, I. & Loubeyre, P. Neutron and X-ray diffraction study of the broken symmetry phase transition in solid deuterium. *Nature* **435**, 1206–1209 (2005).
30. Geneste, G., Torrent, M., Bottin, F. & Loubeyre, P. Strong isotope effect in phase II of dense solid hydrogen and deuterium. *Phys. Rev. Lett.* **109**, 155303 (2012).
31. Loubeyre, P., Occelli, F. & Dumas, P. Hydrogen phase IV revisited via synchrotron infrared measurements in H_2 and D_2 up to 290 GPa at 296 K. *Phys. Rev. B* **87**, 134101 (2013).
32. Zhang, X.-W., Wang, E.-G. & Li, X.-Z. Ab initio investigation on the experimental observation of metallic hydrogen. *Phys. Rev. B* **98**, 134110 (2018).
33. Carbotte, J. P., Nicol, E. J. & Timusk, T. Detecting superconductivity in the high pressure hydrides and metallic hydrogen from optical properties. *Phys. Rev. Lett.* **121**, 047002 (2018).

Methods

The toroidal diamond anvil cell

The toroidal shape of the synthetic single-crystal diamond anvil tip was prepared by focused ion beam machining. Scanning electron micrograph and profile of the toroidal tip are given in Extended Data Fig. 6. The central flat diameter, groove and depth are 25 μm, 80 μm and 4.6 μm, respectively. The toroidal tip has been recovered intact upon full pressure release, indicating its purely elastic deformation up to the highest pressure reached. That indicates that no irreversible transformation of the anvil at tip in contact with the hydrogen sample has perturbed the absorption measurements. Breakage on the bevelled slope of the anvil is observed, as in standard DAC, but outside of the focused ion beam-machined central part.

High pressures were generated using the T-DAC, consisting of a LeToullec membrane diamond anvil cell equipped with Boehler–Almax type seats of polycrystalline diamond and equipped with toroid-shaped diamond anvils. The hydrogen sample was loaded in the T-DAC under a pressure of 140 MPa. A focused ion beam-drilled rhenium gasket was used. The sample pressure was slowly increased to enable the gradual elastic deformation of the anvil tip by changing the membrane pressure pushing the piston with a rate of 0.2 bar min^{-1}. The red colour of the diamond tip is gradually observed above 350 GPa, reversibly disappearing upon pressure release, owing to the diamond bandgap closing within the visible range at the diamond tip[8,34].

The sample thickness, 1.6 ± 0.1 μm, was estimated by the conservation of the hydrogen mass between loading (33.6 cm^3 mol^{-1} of hydrogen loaded in a gasket hole 14 μm in diameter and 6 μm thick) and the sample at 400 GPa (1.6 cm^3 mol^{-1} in a diameter of about 5.8 ± 0.2 μm).

The conversion between the membrane pressure, P_m, and the force on the piston, F, is F [kN] = 0.05 × P_m [bar].

Pressure measurement

The high-frequency step of the T_{2g} Raman spectra of the stressed diamond anvil was used to measure the pressure at the hydrogen sample. The hydrogen sample pressure is related to the diamond-edge wavenumber by the Akahama calibration[35]. The revision[36] of this calibration curve up to the 400 GPa pressure range was discarded because the pressure appeared to be overestimated, on the basis of the following: (1) in our previous measurements with toroidal anvils using X-ray diffraction[8], the rhenium pressure gauge gave values in better agreement with the original pressure scale; (2) as seen in Extended Data Fig. 7, the pressure evolution versus the membrane pressure and the infrared vibron wavenumber versus pressure exhibit unphysical behaviours when using the revised scale; and (3) the revised scale is based on the Pt equation of state[37] that has been recently shown to overestimate pressure[38]. The pressure of the bandgap data measured previously in the visible range[18] has been corrected using the same pressure calibration as in the present study (−20 GPa). No difference up to a pressure of 330 GPa, estimated with the diamond-edge Raman pressure gauge, could be observed between operating the toroidal anvils or the standard bevelled anvils, by looking at the infrared H_2 vibron wavenumber versus pressure (see Extended Data Fig. 3). The error bars in the pressure measurements, ±10 GPa, arise from the random uncertainties originating from the positional accuracy of the sample and the stress field at the tip. The systematic uncertainties owing to the pressure calibration scale are not taken into account. The estimated pressures may be corrected in the future if the diamond-edge pressure gauge calibration is refined. The pressure scale used here is:

$$P[\mathrm{GPa}] = 547\frac{\Delta\omega}{\omega_0}\left(1+1,375\frac{\Delta\omega}{\omega_0}\right)$$

where $\Delta\omega$ is the frequency shift of the diamond edge and ω_0 = 1,334 cm^{-1}.

Infrared bench

A photograph of the bench is shown in Extended Data Fig. 8. This bench was previously used to characterize the infrared vibrational modes of phase IV of hydrogen at 300 K[31]. The custom-made horizontal infrared microscope is equipped with two infinity-corrected long-working-distance Schwarzschild objectives (working distance, 47 mm; numerical aperture, 0.5; magnification, 15×) that produce a 23 μm (full width at half maximum, FWHM) infrared spot at a wavelength of 10 μm. This beam size is reduced inside the T-DAC owing to the effect of the diamond refractive index. The spatial and temporal stability of the broadband infrared beam enabled us to record transmission spectra, with a good signal-to-noise ratio over the range 800–8,000 cm^{-1} for a hole of diameter 6 μm (see Extended Data Fig. 8). One of the Schwarzschild objectives is mounted on a 300-mm translation stage to free up space behind the cryostat in order to insert the optical head for Raman spectroscopy measurements without moving the T-DAC. The Raman signal was excited by a 660-nm-wavelength laser limited to 3 mW power output above 300 GPa to prevent thermal heating and hence breakage of the toroidal tip. The Raman head is also equipped with a digital camera to take photographs of the sample at each pressure. The quality of the measurements obtained also relies on the high mechanical stability of the bench and on the high reproducibility in position upon swapping between the infrared and the Raman configurations. Infrared spectra were collected with a 4 cm^{-1} resolution and 1,024 scans, with an electron beam current of 450 mA (top-up mode).

Absorption spectra

All spectra were recorded using the transmission geometry and then divided by a reference transmission spectrum, here taken at 123 GPa. Such a pressure is high enough to avoid any Fabry–Perot interference signal coming from the two parallel diamond interfaces of high refractive index enclosing the sample, but with the absence of the strong H_2 vibron absorption which appears above 160 GPa in phase III. The overall intensity (peak-to-peak value of the interferogram) of the spectra has been normalized by that at 310 GPa to take into account the change in the hydrogen sample diameter owing to its compression. It was observed that above 310 GPa, the sample size is almost constant upon pressure increase and decrease. The absorbance is defined as $A = -\log_{10}(I(\upsilon)/I_0(\upsilon))$, where I is the intensity of the raw spectrum at a frequency υ.

In the present experimental configuration, the maximum absorbance value that could be reasonably measured is approximately 2, indicating that less than 1% of the reference spectrum signal is detected. Considering the small gasket hole, the detection of the signal remained challenging and required using the detector gain at maximum value, inducing an increase of the intrinsic detector noise.

Data availability

The data that support the findings of this study are available from the corresponding author upon request.

34. Ruoff, A. L., Luo, H. & Vohra, Y. K. The closing diamond anvil optical window in multimegabar research. *J. Appl. Phys.* **69**, 6413–6416 (1991).
35. Akahama, Y. & Kawamura, H. Pressure calibration of diamond anvil Raman gauge to 310 GPa. *J. Appl. Phys.* **100**, 043516 (2006).
36. Akahama, Y. & Kawamura, H. Pressure calibration of diamond anvil Raman gauge to 410 GPa. *J. Phys. Conf. Ser.* **215**, 012195 (2010).
37. Holmes, N. C., Moriarty, J. A., Gathers, G. R. & Nellis, W. J. The equation of state of platinum to 660 GPa. *J. Appl. Phys.* **66**, 2962–2967 (1989).
38. Yokoo, M., Kawai, N., Nakamura, K. & Kondo, K. Ultrahigh-pressure scales for gold and platinum at pressures up to 550 GPa. *Phys. Rev. B* **80**, 104114 (2009).
39. Ishmaev, S. N. et al. Neutron structural investigations of solid parahydrogen at pressures up to 24 kbar. *Sov. Phys. JETP* **84**, 394–403 (1983).
40. Dewaele, A., Torrent, M., Loubeyre, P. & Mezouar, M. Compression curves of transition metals in the Mbar range: experiments and projector augmented-wave calculations. *Phys. Rev. B* **78**, 104102 (2008).
41. Vinet, P., Ferrante, J., Rose, J. H. & Smith, J. R. Compressibility of solids. *J. Geophys. Res.* **92**, 9319–9325 (1987).

42. Akahama, Y. et al. Evidence from X-ray diffraction of orientational ordering in phase III of solid hydrogen at pressures up to 183 GPa. *Phys. Rev. B* **92**, 060101 (2010).
43. Zha, C.-S., Liu, Z. & Hemley, R. J. Synchrotron infrared measurements of dense hydrogen to 360 GPa. *Phys. Rev. Lett*. **108**, 146402 (2012).

Acknowledgements We thank O. Marie for focused ion beam machining the toroidal anvils and the gasket holes. We are grateful to the SOLEIL director general, J. Daillant, for giving us regular access to the infrared beamline over the past six years. The inputs of S. Lefrançois in designing and assembling the horizontal infrared microscope and of the optics group at SOLEIL in aligning the Schwarzschild objectives are appreciated. We thank F. Borondics and F. Capitani for their assistance at the SMIS beamline.

Author contributions P.L. designed the project. P.L. and F.O. prepared and loaded the T-DAC. P.D., F.O. and P.L. developed the infrared microscope. P.L., F.O. and P.D. conducted the experiment and analysed the data. P.L. and P.D. wrote the manuscript. All authors discussed the results.

Competing interests The authors declare no competing interests.

Additional information

Supplementary information is available for this paper at https://doi.org/10.1038/s41586-019-1927-3.

Correspondence and requests for materials should be addressed to P.L.

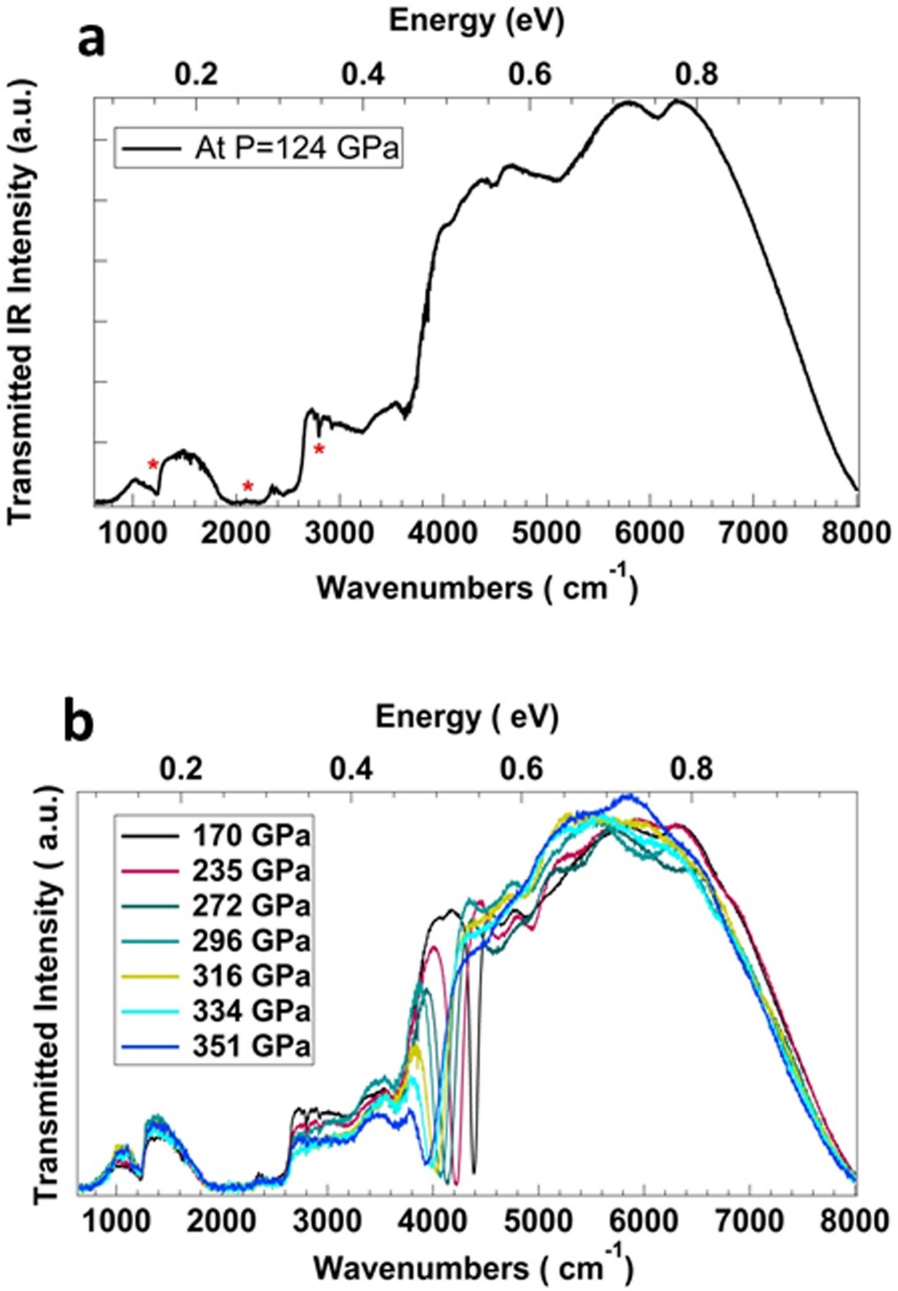

Extended Data Fig. 1 | Infrared spectra below 350 GPa. a, Single-beam spectrum at 123 GPa, used as the reference spectrum for the absorption spectra. The three red stars indicate parasitic effects corresponding to, from right to left, absorption peaks of impurities around 2,800 cm^{-1}, a broad absorption band from the diamond (1,900–2,300 cm^{-1}), and a broad absorption around 1,200 cm^{-1} from the protected layers of the aluminium mirrors of the beamline. **b**, Single-beam spectra, after intensity normalization (peak-to-peak value of their respective interferogram before Fourier transform). IR, infrared.

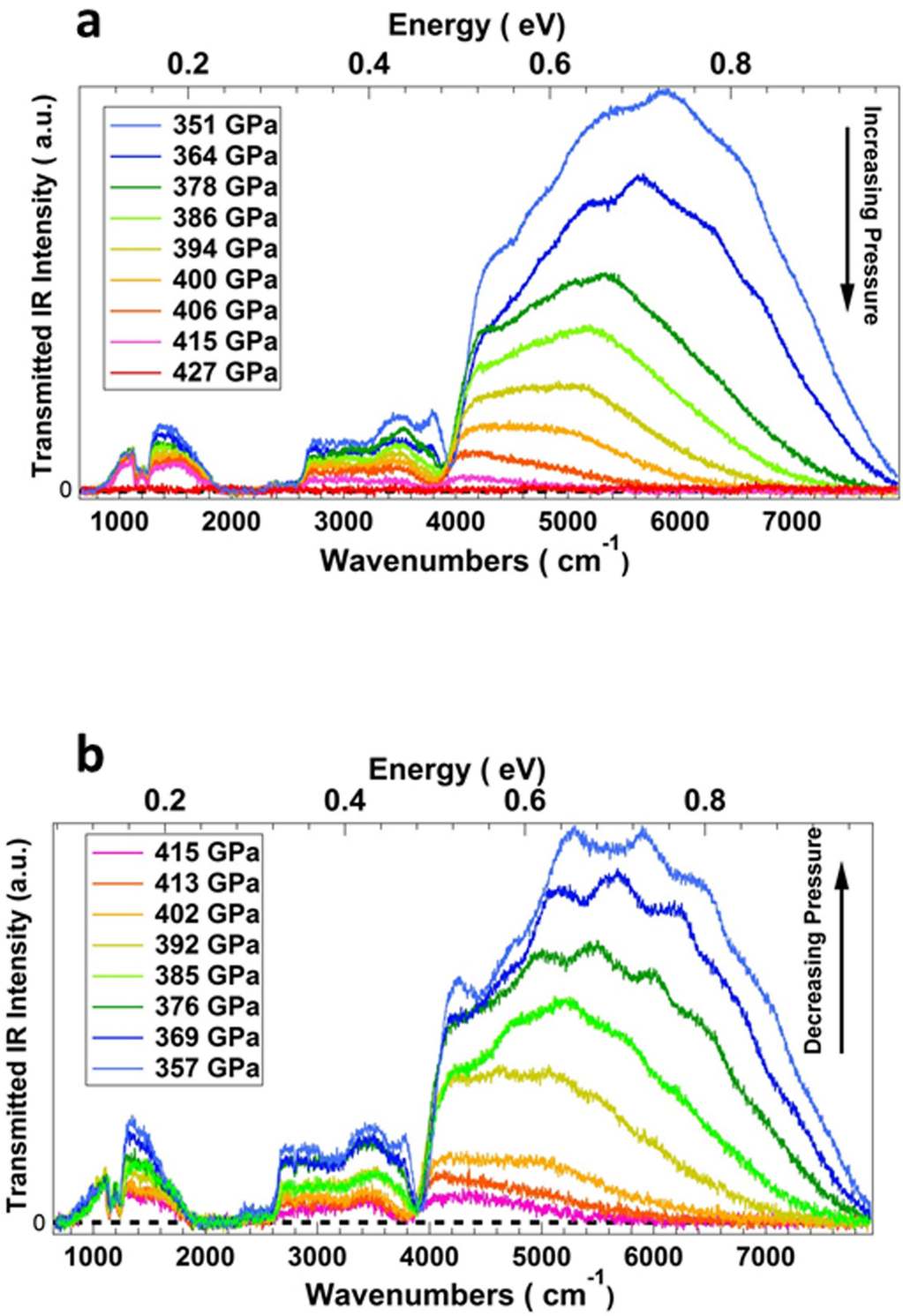

Extended Data Fig. 2 | Infrared spectra above 350 GPa with pressure increase and pressure decrease. a, **b**, These spectra show a zeroing at high wavenumbers, progressing towards low wavenumber values with pressure increase (**a**) and reversibly, to the opposite direction upon pressure release (**b**).

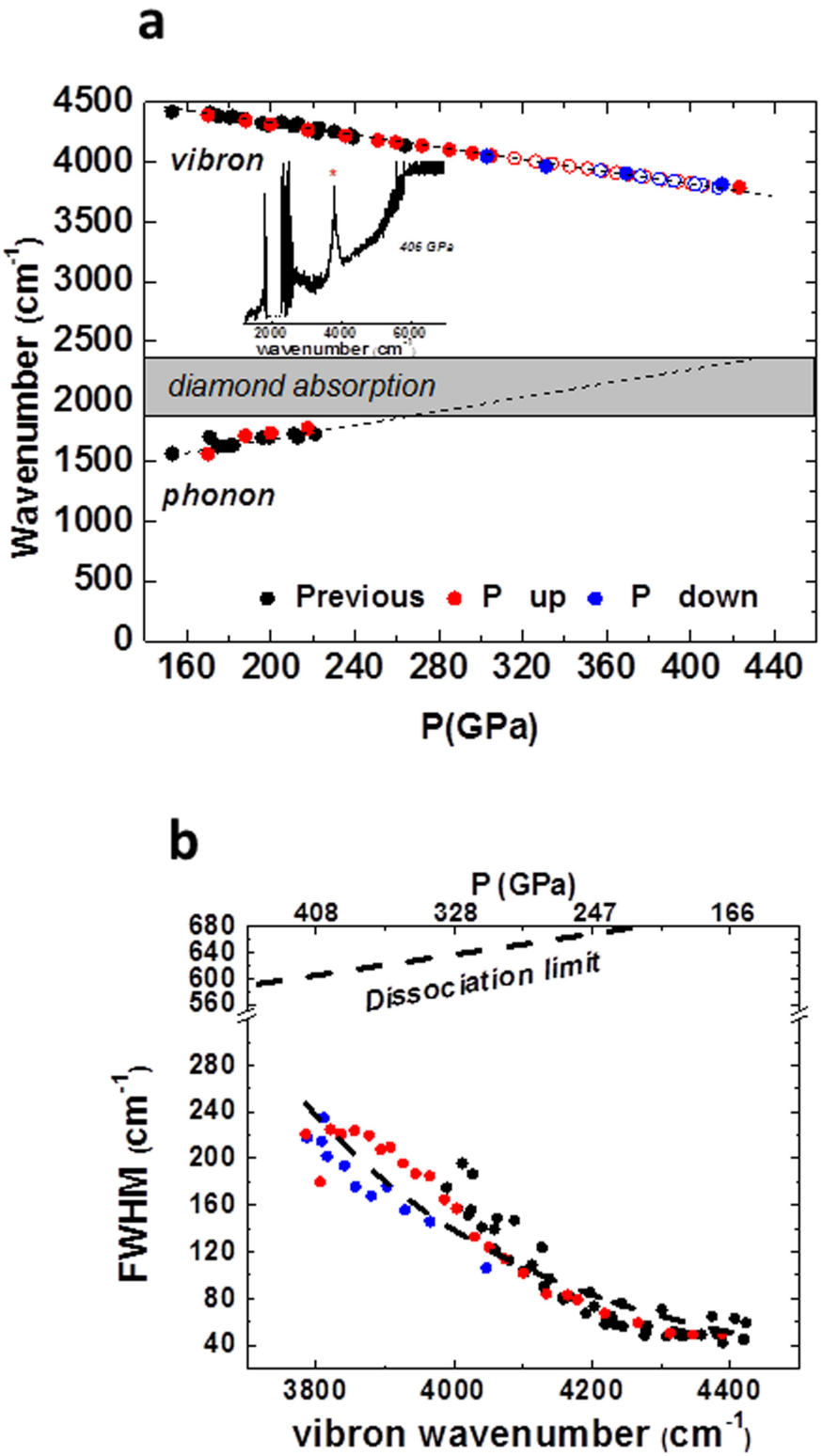

Extended Data Fig. 3 | Infrared vibron and phonon wavenumbers versus pressure. a, The symbols indicate: red, pressure increase; blue, pressure decrease; and black, previous work performed using standard diamond anvil cells. The filled dots indicate the pressure measured by the diamond pressure scale and the open symbols are the position according to the linear vibron shift as a function of pressure. Inset, infrared spectrum at 406 GPa, in arbitrary absorbance units, with the vibron peak indicated by a red star. The linear fit of the vibron wavenumber with pressure is given by: $\upsilon_{\mathrm{vibron}}\,[\mathrm{cm}^{-1}] = 4{,}814 - 2.48P\,[\mathrm{GPa}]$ and that of the phonon wavenumber by: $\upsilon_{\mathrm{phonon}}\,[\mathrm{cm}^{-1}] = 1{,}163 + 2.69P\,[\mathrm{GPa}]$. **b**, FWHM of the vibron peak versus its wavenumber, $\upsilon_{\mathrm{vibron}}$. The increase in the vibron linewidth with pressure remains well below the dissociation limit value, given by FWHM = $E/2\pi$, with $E = h\upsilon_{vibron}$ the vibron energy and where h is the Planck constant. This limit is estimated by assuming that the lifetime of the vibron state (inferred by assuming it is the only contribution to the line broadening) is equal to the vibration period.

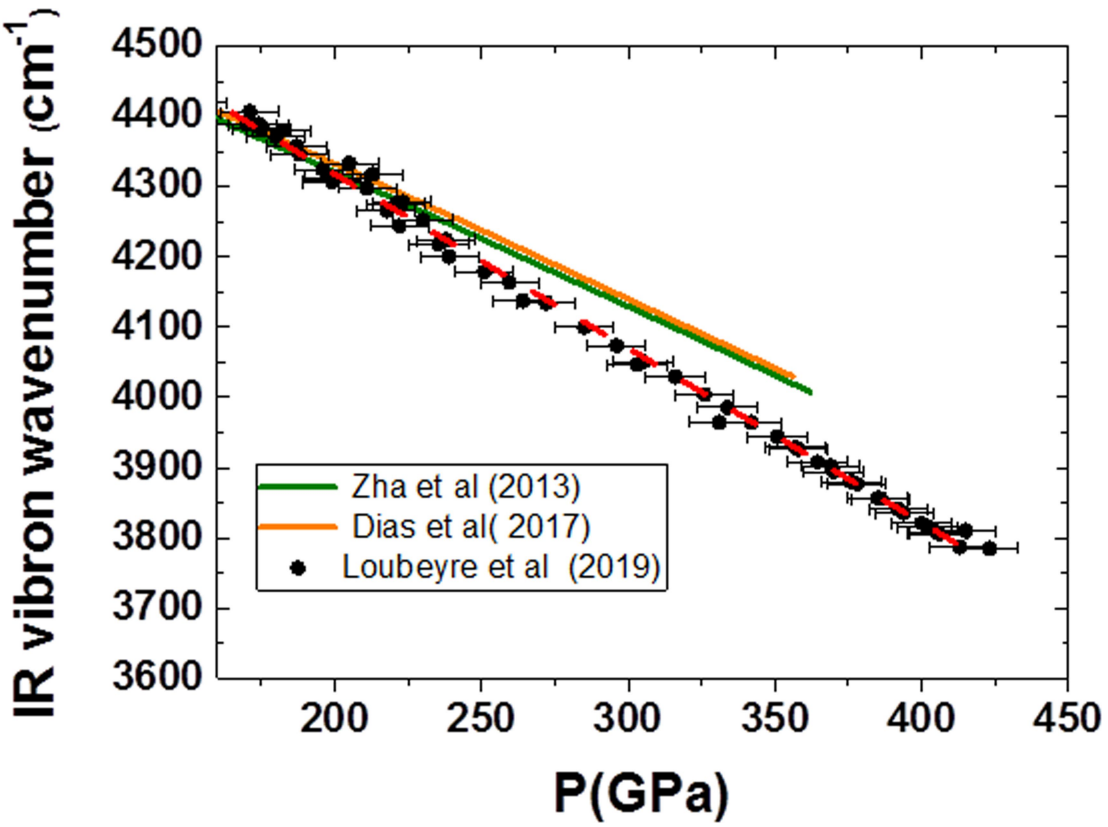

Extended Data Fig. 4 | Infrared vibron wavenumber versus pressure. The present data (black dots), and their linear fit (red dashed line) are compared to the linear fits of previous measurements[7,43] up to 360 GPa. Pressure uncertainty is ±10 GPa.

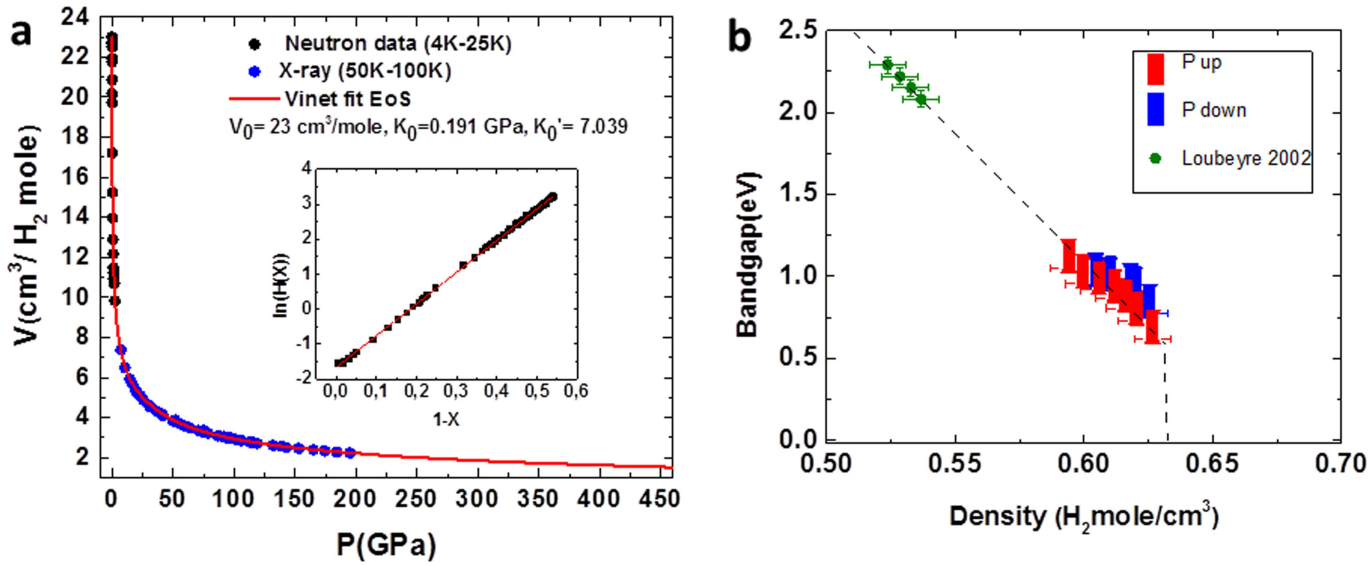

Extended Data Fig. 5 | Hydrogen equation of state and evolution of the direct electronic bandgap versus density. a, Equation of state of solid hydrogen around 80 K. The black dots are neutron diffraction measurements[39]. The blue dots are our unpublished X-ray diffraction data obtained at the European Synchrotron Radiation Facility; the pressure scale is based on the revised ruby scale[40]. The red line is the fit of the experimental data by a Vinet form[41]: $P = 3K_0(1-X)X^{-2}\exp[3/2(K_0'-1)(1-X)]$, with $X = (V/V_0)^{1/3}$, $K_0 = 0.191$ GPa, $K_0' = 7.039$ (where $K_0' = dK_0/dP$), and $V_0 = 23$ cm^3 mol^{-1}. The present equation of state is in good agreement with that measured previously[42]. Inset, the Vinet form can be reformulated in terms of expressions analogous to normalized stress, $\ln[H(X)] = \ln[PX^2/3(1-X)]$, and Eulerian strain, $(1-X)$. This gives: $\ln[H(X)] = \ln K_0 + 3/2(K_0'-1)(1-X)$. The linear fit of the data is shown. **b**, Evolution of the direct bandgap of solid hydrogen with density, for pressure increase (red), pressure decrease (blue) and from a previous study in the visible range[18] (green). The vertical rectangles indicate the maximum 0.14-eV underestimation of the bandgap owing to the limited absorbance value of 2 that could be measured. The density uncertainties (±0.007 H_2 mole cm^{-3}) are obtained by propagating the ±10 GPa pressure uncertainties.

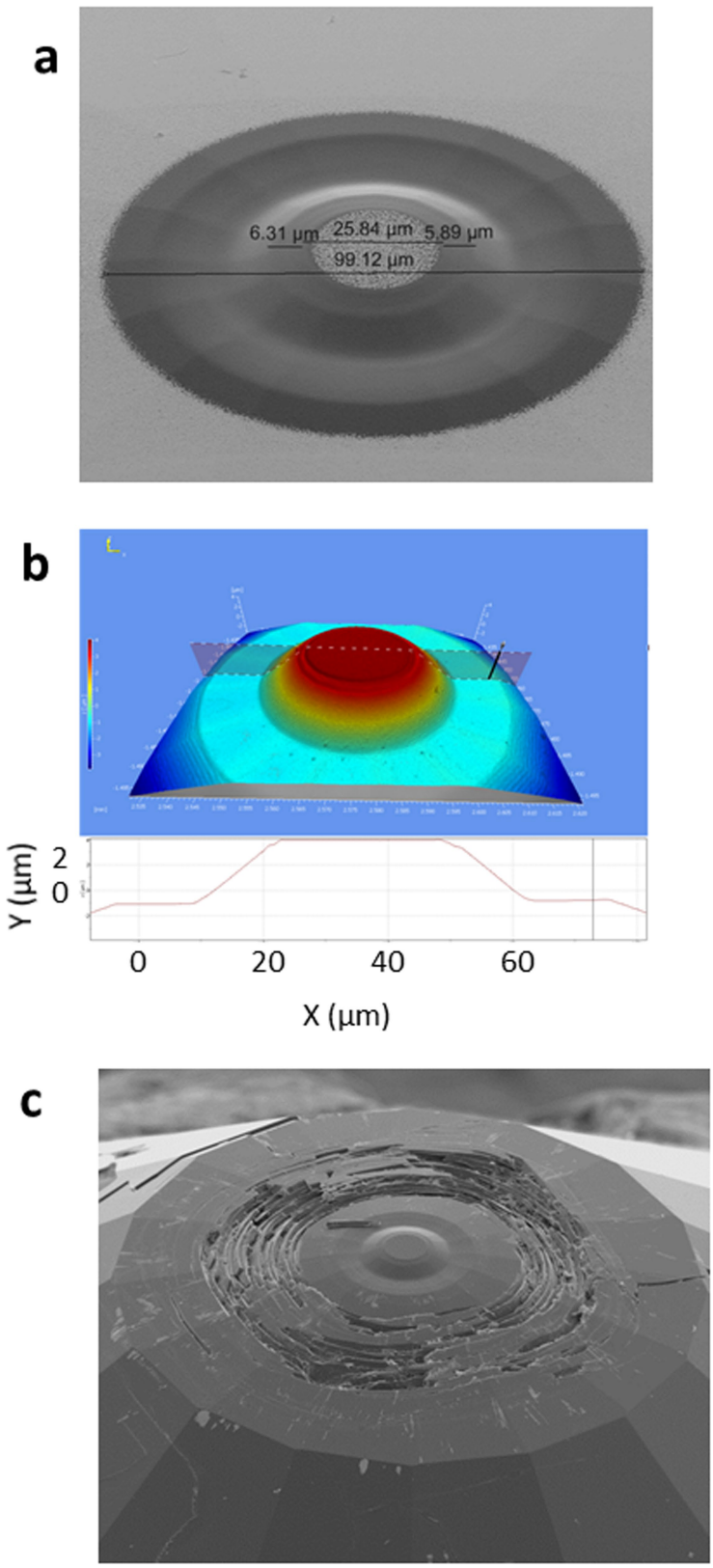

Extended Data Fig. 6 | Geometry of the toroidal shape. a, Scanning electron micrograph of the anvil. **b**, Profile of the toroidal diamond tip measured by interferometry. **c**, Scanning electron microscope image of the toroidal anvil recovered after pressure release. The toroidal part of the anvil is intact. Ring cracks are seen on the bevel of the anvil, at a diameter of about 150 µm.

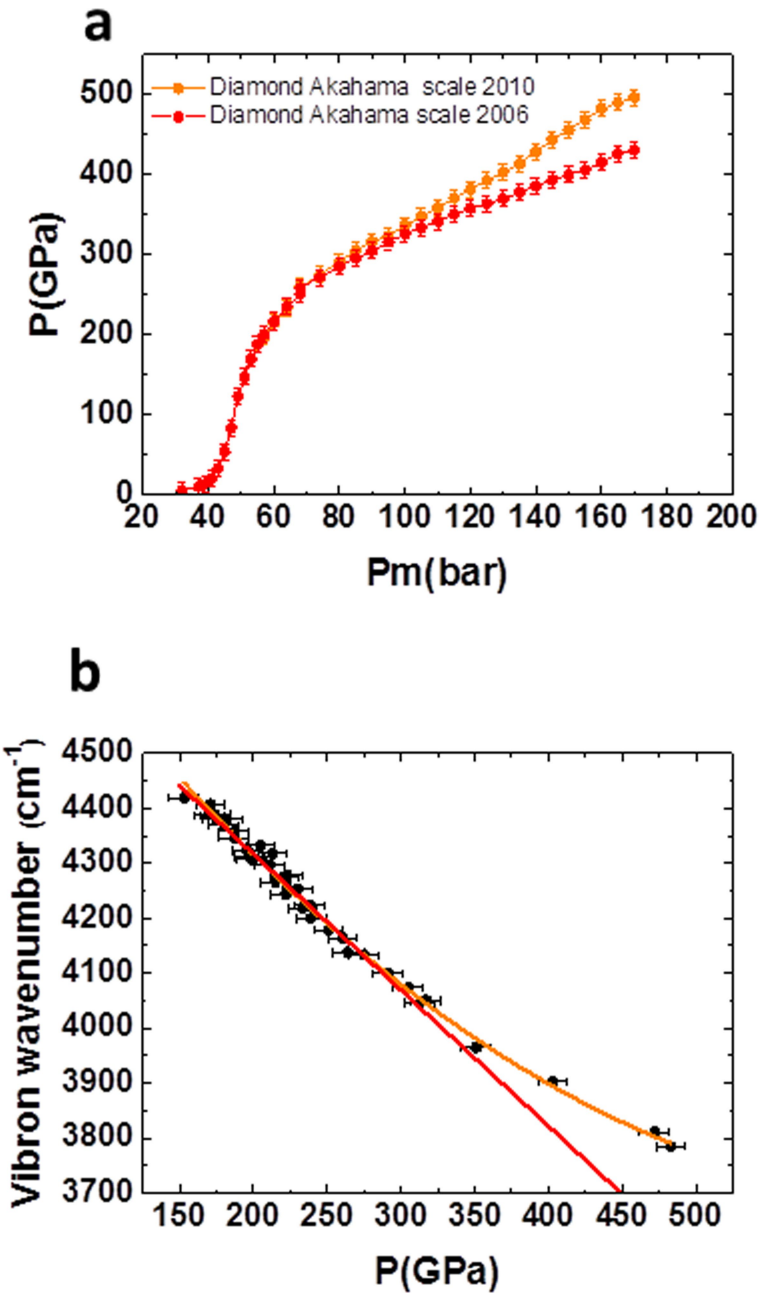

Extended Data Fig. 7 | Comparison of the original[35] and revised[36] Akahama diamond pressure scales for two measurements. The two scales deviate above 300 GPa. **a**, Sample pressure–load curve. The force on the piston of the T-DAC is linearly related to the helium gas pressure inflating the membrane, F [kN] = 0.05 × P_m [bar]. The revised scale (orange) gives a convex evolution above 300 GPa that is mechanically incorrect. **b**, Infrared H_2 vibron wavenumber versus pressure. Above 300 GPa, using the original scale (red), the shift is linear, in agreement with the calculated trend in phase III[22,25]; however, using the revised scale (dots and orange line), a sublinear shift is observed. The error bars in the pressure measurements (±10 GPa) arise from the random uncertainties originating from the positional accuracy of the sample and the stress field at the diamond anvil tip.

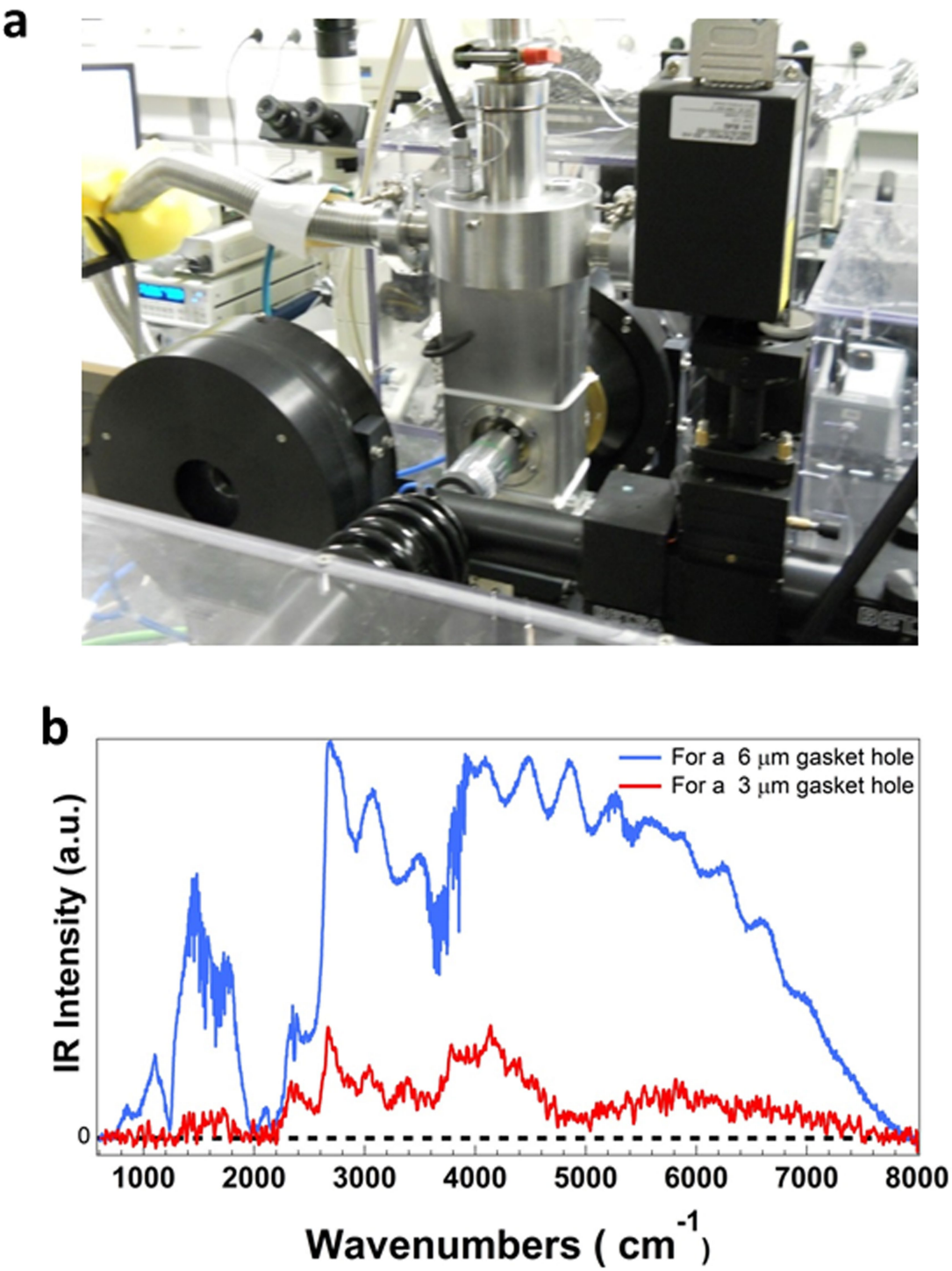

Extended Data Fig. 8 | Experimental setup on the horizontal infrared microscope at the SMIS beamline of the SOLEIL synchrotron. a, The L–N_2 flow cryostat containing the T-DAC sits between the two Schwarzschild objectives for infrared transmission measurements. In the Raman configuration, one of the Schwarzschild objectives is swapped by the Raman head. Both configurations are reproducibly recovered within about 2 μm, because they are mounted on a precise, long-travel translation stage. **b**, Raw spectra recorded through two calibrated gasket holes 6 μm and 3 μm in diameter, made by focused ion beam machining in a rhenium gasket, and positioned between the two diamond anvils of the T-DAC. The spectra were recorded with a resolution of 4 cm^{-1} and after 400 accumulations.

Extended Data Table 1 | Infrared vibron wavenumber, direct bandgap and corresponding pressure

a

Vibron H2 (cm^{-1})	Energy gap(eV)	P (GPa)
3894	1.05 (+0.14)	370
3877	0.95 (+0.14)	378
3856	0.90 (+0.14)	386
3836	0.87 (+0.14)	394
3821	0.80 (+0.14)	400
3806	0.73 (+0.14)	406
3785	0.62 (+0.14)	415

b

Vibron H2 (cm^{-1})	Energy gap(eV)	P (GPa)
3787	0.77 (+0.14)	413
3808	0.87 (+0.14)	405
3816	0.90 (+0.14)	402
3841	0.94 (+0.14)	392
3857	0.96 (+0.14)	385

The pressure uncertainty is ±10 GPa, the bandgap uncertainty is +0.14 eV and the vibron wavenumber uncertainty is ±4 cm^{-1}. Top, increasing pressure; bottom, decreasing pressure.